

Constraining Self-Interacting Dark Matter with Dwarf Spheroidal Galaxies and High-resolution Cosmological N -body Simulations

Toshihiro Ebisu

*Department of Applied and Cognitive Informatics, Chiba University,
1-33, Yayoi-cho, Inage-ku, Chiba 263-8522, Japan*

Tomoaki Ishiyama*

*Institute of Management and Technologies, Chiba University,
1-33, Yayoi-cho, Inage-ku, Chiba 263-8522, Japan*

Kohei Hayashi

*National Institute of Technology, Ichinoseki College,
Takanashi, Hagisho, Ichinoseki, Iwate, 021-8511, Japan*

(Dated: January 3, 2022)

We study the density structures of dark matter subhalos for both cold dark matter and self-interacting dark matter models using high-resolution cosmological N -body simulations. We quantify subhalo's central density at 150 pc from the center of each subhalo at the classical dwarf spheroidal and ultrafaint dwarf scales found in Milky-Way sized halos. By comparing them with observations, we find that the self-interacting scattering cross-section of $\sigma/m < 3 \text{ cm}^2\text{g}^{-1}$ is favored. Due to the combination of hosts' tide and self-interactions, the central density of subhalos with small pericenter shows a noticeable difference between the cold and the self-interacting models, indicating that Milky-Way satellites with small pericenter are ideal sites to further constrain the nature of dark matter by future large spectroscopic surveys.

I. INTRODUCTION

The cold dark matter (CDM) model, which assumes collisionless dark matter particles, has successfully reproduced the structure of the Universe on large scales ($\geq 1 \text{ Mpc}$) [1–7]. However, on smaller scales, especially on dwarf galaxies, discrepancies exist between observations and CDM predictions, called the “small scale crisis”. For example, cosmological N -body simulations based on the CDM predict cuspy density profiles of dark matter halos [8], whereas observations of dwarf galaxies suggest cored profiles [9–12]. This discrepancy is known as the core-cusp problem and has recently been reinterpreted as the diversity problem [13]: circular velocity profiles of observed dwarf galaxies show a large diversity even with similar maximum circular velocity. Some dwarf galaxies have cuspy profiles, and others have cored profiles, whereas those simulated galaxies show little variation. Baryonic physics in galaxies can be a solution to this problem although their effects are still uncertain.

Self-interacting dark matter (SIDM) models [14] have been proposed to solve the small scale crisis (for a review, see [15]). The original SIDM assumes that the scattering cross-section of dark matter particles per unit mass, σ/m , is velocity-independent and isotropic. However, preferred cross-sections are different depending on scales: $\sigma/m \gtrsim 1 \text{ cm}^2\text{g}^{-1}$ for dwarf galaxies [16–18] and $\sigma/m \lesssim 0.1\text{--}1 \text{ cm}^2\text{g}^{-1}$ for galaxy clusters [18–21]. To overcome this hurdle, reincarnations of the original SIDM

have been considered, such as velocity-dependent SIDM (e.g., [22–26]) and SIDM with anisotropic scattering from the approach of particle physics (e.g., [27–29]).

Dark matter self-interaction decreases the central density of halos before gravothermal core-collapse sets in [30, 31]. Baryonic physics in galaxies, such as supernova feedback and star formation burst, could also affect the central structures of halos. These two different mechanisms can coincide and interplay. To remove this degeneracy, it is ideal for studying dark matter dominated systems such as classical dwarf spheroidal (dSph) and ultrafaint dwarf (UFD) galaxies. Cosmological hydrodynamical simulations predict that central structures of those host halos are less affected by feedback processes [32–34], maybe because most of the stars in those system were born before the cosmic reionization.

Only recently, the density structures of UFDs have been estimated, and the SIDM cross-section is constrained by them [35]. However, a phenomenological semi-analytic SIDM halo model is used in that study because there is a significant lack of high-resolution simulations for UFD scale subhalos. Semi-analytic models have been used to predict density structures of isolated halos using various SIDM models [35–39], and have the advantage of including baryonic potential and being less computational cost than cosmological simulations. However, in semi-analytic models, it is challenging to model the dynamical evolution of subhalos within a host halo, such as tidal interactions with host halos and other subhalos, and evolution of host halos. Cosmological simulations have the advantage that all these dynamical effects are naturally included.

This paper will revisit the SIDM cross-section using

* e-mail:ishiyama@chiba-u.jp

high-resolution cosmological N -body simulations based on both CDM and SIDM, and observations of the classical dSphs and the UFDs. Unlike previous studies that focused on the diversity of circular velocity profiles (e.g., [40]), we focus on density structures of the classical dSph and the UFD scales subhalos. We quantify the central density at 150 pc, $\rho(150\text{pc})$, from the center of each subhalo and compare them with observations. Read et al. [41] argued that $\rho(150\text{pc})$ is a good tracer of the central density of dwarf galaxies because it is insensitive to the prior choice of the inner slope of the density profile and shows enough difference to distinguish whether the density profile is cusp or cored. Uncertainty in $\rho(150\text{pc})$ is not prohibitively large, and 1σ uncertainty is typically less than 50% for the classical dSphs [41]. The major source of uncertainty is poor observed sample size, thus, future spectroscopic surveys can improve the uncertainty. We also study the dependence of central density on the pericenter distance; It has been pointed out that the dSph's central density $\rho(150\text{pc})$ anti-correlates with the pericenter radii [42, 43].

This paper is organized as follows. In Section II, we explain the details of our cosmological N -body simulations. In Section III and IV, we show and discuss the results. Finally, we present the conclusions in Section V.

II. SIMULATIONS

We performed three high-resolution cosmological N -body simulations: CDM (without self-interaction), SIDM₁ ($\sigma/m = 1 \text{ cm}^2 \text{ g}^{-1}$), and SIDM₃ ($\sigma/m = 3 \text{ cm}^2 \text{ g}^{-1}$). All of the simulations consist of 1024^3 dark matter particles with a particle mass of $4.1 \times 10^4 h^{-1} \text{ M}_\odot$ in a comoving cubic box with a side length of $8 h^{-1} \text{ Mpc}$. We constructed an initial condition using 2LPTIC code [44], and the adopted cosmological parameters are $\Omega_0 = 0.31$, $\Omega_b = 0.048$, $\lambda_0 = 0.69$, $h = 0.68$, $n_s = 0.96$, and $\sigma_8 = 0.83$, which match with observational results by the Planck [45]. We used the same initial condition and numerical parameters for three simulations, in which only the strength of self-interactions is different.

To follow the gravitational evolution of dark matter particles, we used a massively parallel TreePM code, GREEM¹ [46, 47], on the Aterui-II supercomputer at the Center for Computational Astrophysics, National Astronomical Observatory of Japan. The gravitational softening length is $100 h^{-1} \text{ pc}$. We accelerated the tree force calculation by the PHANTOM-GRAPE² software [48–51]. We performed all simulations from redshift $z = 127$ to 0 and stored snapshots covering $z = 12$ to 0 with a logarithmic interval $\Delta \log(1+z) = 0.01$, resulting in a total

of 112 snapshots. We adopted the same algorithm used in Vogelsberger et al. [23] for the implementation of dark matter self-interaction, in which isotropic, velocity independent, and elastic scattering are considered. We do not consider velocity-dependent SIDM models because we focus on scales smaller than galaxies. In Appendix, we compare the core size of the host halos with a previous study to show the validity of our SIDM implementation.

We identified gravitationally bound dark matter halos and subhalos using ROCKSTAR halo/subhalo finder [52] and constructed merger trees using CONSISTENT TREES merger tree code [53]. We unbiasedly picked out nine Milky Way-sized host halos (H0-H8) covering the virial mass range of 3.4×10^{11} to $2.8 \times 10^{12} h^{-1} \text{ M}_\odot$. The virial mass M_{vir} and radius R_{vir} of each halo are summarized in Table I. We analyzed their subhalos more massive than $1.0 \times 10^8 h^{-1} \text{ M}_\odot$, which consists of more than 2,400 particles and corresponds to the massive UFD scale.

III. RESULTS

A. Central density of subhalos

Fig. 1 shows the relation between the subhalos' density at 150 pc, $\rho(150\text{pc})$, and their pericenter radii r_{peri} . We can not directly measure $\rho(150\text{pc})$ from our simulations because the softening length adopted is $100 h^{-1} \text{ pc}$ ($= 147 \text{ pc}$). Therefore, we estimate $\rho(150\text{pc})$ by fitting the density profiles of the subhalos with the NFW profile [8] expressed by

$$\rho_{\text{NFW}}(r) = \frac{\rho_s r_s^3}{r(r_s + r)^2}, \quad (1)$$

and with the Burkert profile [9] expressed by

$$\rho_B(r) = \frac{\rho_b r_b^3}{(r + r_b)(r^2 + r_b^2)}. \quad (2)$$

We use the NFW profile for the CDM simulation and the Burkert profile for the SIDM₁ and SIDM₃ simulations. The fittings were performed using up to 20 bins covering $0.01 R_{\text{vir}} \leq r \leq R_{\text{vir}}$, and only bins with $r > 300 \text{ pc}$ were used. We also calculated the pericenter of each subhalo as the minimum distance from its host over the subhalo's history. The nine pericenter bins cover $10 \text{ kpc} \leq r_{\text{peri}} < 190 \text{ kpc}$ at equally spaced intervals.

We compare simulated $\rho(150\text{pc})$ with the observation. We use $\rho(150\text{pc})$ of observed classical dSphs and UFDs that were estimated by [43] and Hayashi et. al. (in prep.), respectively. To compute $\rho(150\text{pc})$, they determined a dark matter density profile by non-spherical dynamical models based on axisymmetric Jeans equations. They applied these models to the line-of-sight velocity data for the dSphs and UFDs and obtained the posterior distribution functions for the dark matter halo parameters (see [43] in details). Thus, the estimated $\rho(150\text{pc})$ were marginalized by all these parameters.

¹ <https://hpc.imit.chiba-u.jp/~ishiytm/greem/>

² <https://bitbucket.org/kohji/phantom-grape/src>

TABLE I. Virial mass M_{vir} and radius R_{vir} of nine Milky Way-sized host halos.

	CDM		SIDM ₁		SIDM ₃	
Name	M_{vir}	R_{vir}	M_{vir}	R_{vir}	M_{vir}	R_{vir}
	$[10^{11} h^{-1} \text{M}_{\odot}]$	$[h^{-1} \text{kpc}]$	$[10^{11} h^{-1} \text{M}_{\odot}]$	$[h^{-1} \text{kpc}]$	$[10^{11} h^{-1} \text{M}_{\odot}]$	$[h^{-1} \text{kpc}]$
H0	25.76	278.6	25.65	278.2	24.94	275.6
H1	11.08	210.3	11.04	210.0	10.97	209.6
H2	10.56	206.9	10.51	206.6	10.37	205.7
H3	8.105	189.4	7.920	188.0	7.687	186.2
H4	7.141	181.7	7.097	181.2	7.033	180.7
H5	6.902	179.6	6.861	179.3	6.795	178.7
H6	6.800	178.7	6.873	179.4	6.732	178.1
H7	4.581	156.7	4.520	156.0	4.435	155.0
H8	3.755	146.6	3.556	144.0	3.463	142.7

Fig. 1 (top row) shows that the central density $\rho(150\text{pc})$ of subhalos in the CDM simulation is in good agreement with those of the classical dSphs and anti-correlates with the pericenter r_{peri} , consistent with observational results [42, 43]. On the other hand, the density $\rho(150\text{pc})$ of subhalos in the SIDM simulations is systematically lower than CDM counterparts and the classical dSphs. The central density does not depend strongly on the pericenter and is lower in the SIDM₃ than in the SIDM₁. The difference with the classical dSphs is also larger in the SIDM₃. These results indicate that the SIDM scattering cross section of $\sigma/m < 1 \text{ cm}^2\text{g}^{-1}$ is favored.

The bottom row of Fig. 1 shows the comparison with the UFDs. Unlike the classical dSphs, the central density $\rho(150\text{pc})$ estimated in the observed UFDs does not clearly depend on the pericenter, although observational uncertainty is large. Within the first and third quartiles, none of the three simulations is in good agreement with the observations. In terms of the overall distribution, SIDM₁ shows the best match with the observations. The CDM simulation has difficulty reproducing Boötes 1, although it shows consistency with the others. For a few UFDs, the $\rho(150\text{pc})$ in SIDM₃ is too low compared to the UFDs. These results indicate that the SIDM scattering cross-section of $\sigma/m \lesssim 3 \text{ cm}^2\text{g}^{-1}$ is favored, which is consistent with the indication from the comparison with the classical dSphs.

Fig. 1 also shows that the density $\rho(150\text{pc})$ of subhalos in simulations depend on their V_{peak} , which is the maximum circular velocity over the subhalo's history. Denser subhalos tend to have lower V_{peak} in the SIDM₁ and SIDM₃ simulations, whereas denser subhalos tend to have higher V_{peak} in the CDM simulation. We further investigate these results in the next section.

Our results presented above can be affected by the adopted fitting procedure. To confirm the robustness of the results, we try to fit the subhalo's density profile with

the cuspy profile expressed by

$$\rho_{\text{cuspy}}(r) = \frac{\rho_s r_s^3}{r^\alpha (r_s + r)^{3-\alpha}}. \quad (3)$$

This cuspy profile is the same as the NFW when $\alpha = 1$. The central slope α is a fitting parameter (with the range of $0 < \alpha < 3$), and thus, this profile can be applied for both cuspy and cored profiles. Figure 2 shows the results using the cuspy profile for all three simulations. The fitting procedure has little impact on the density $\rho(150\text{pc})$ in the CDM case. On the other hand, the density $\rho(150\text{pc})$ in the SIDM simulations is systematically higher in the cuspy profile than in the Burkert profile because subhalos can have cores or very shallow cusps (shallower than -1). However, the overall trend between $\rho(150\text{pc})$ and r_{peri} in each simulation is the same as Fig. 1 and 2.

B. Density profile of subhalos

As discussed in the previous section, the central density of subhalos with small pericenter shows a stark difference between the CDM and SIDM simulations. To understand the origin of the difference, we separate subhalos according to the pericenter and compare the density profile of each simulation.

Fig. 3 and 4 show density profiles of subhalos with the pericenter $r_{\text{peri}} < 30\text{kpc}$ and $130 \text{ kpc} \leq r_{\text{peri}} < 150 \text{ kpc}$, respectively, in which the color of each curve is proportional to its V_{peak} . We plot only subhalos with masses between 10^8 and $10^9 h^{-1}\text{M}_{\odot}$. The top and bottom panels show the results of subhalos hosted by H0 and H1, respectively. From left to right, the results for the CDM, SIDM₁, and SIDM₃ simulations are shown. For subhalos with small pericenter ($r_{\text{peri}} < 30\text{kpc}$), the density slopes of the very inner regions are steepest in the CDM than in the SIDM simulations. The logarithmic slope $\frac{d \log \rho}{d \log r}$ is typically -1 for the CDM, between -1 and 0 for the SIDM₁, and ~ 0 (constant density) for the SIDM₃,

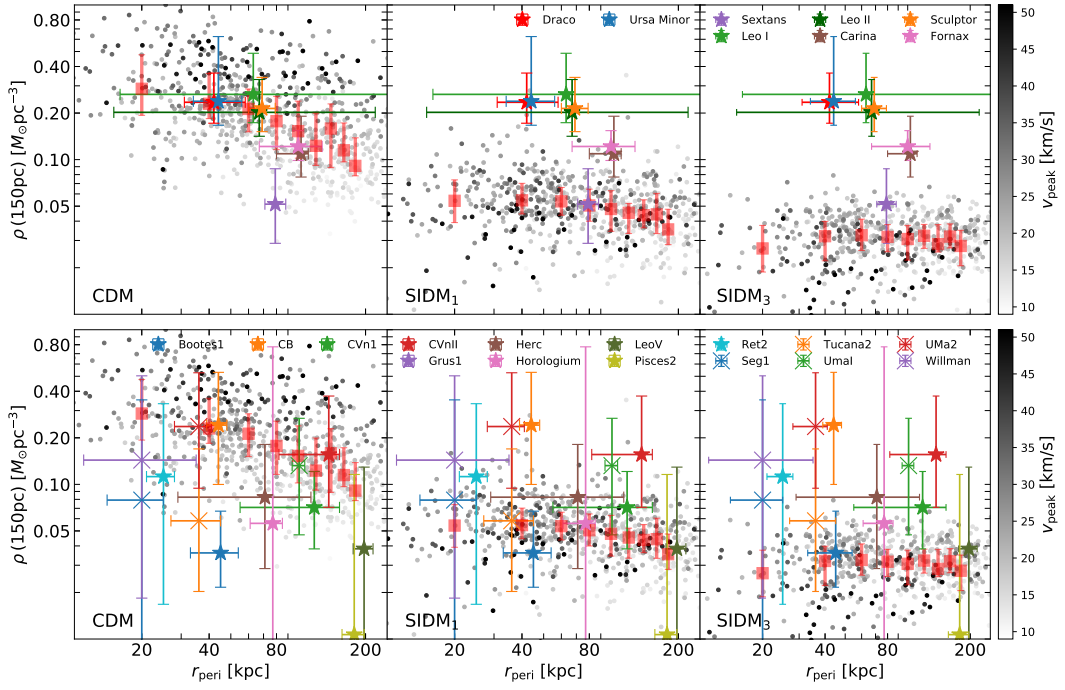


FIG. 1. Subhalos' density at 150 pc, $\rho(150\text{pc})$, versus their pericenter radii, r_{peri} . Color filled stars and crosses with error bars show observational results of the eight classical dSphs [43] (Draco, Ursa Minor, Sextans, Leo I, Leo II, Sculptor, Carina, and Fornax are shown in the upper row) and the 15 UFDs (Boötes, Coma Berenices (CB), Canes Venatici I (CvnI), Canes Venatici II (CvnII), Hercules (Herc), Leo V, Grus 1, Horologium I, Pisces II, Reticulum II (Ret2), Tucana 2, Ursa Major I (UMa1), Ursa Major II (UMa2), Segue 1, and Willman 1 are shown in the bottom row) (Hayashi et. al. (in prep.)). Filled circles are individual subhalos in the nine Milky Way-sized halos in simulations, CDM (left), SIDM_1 (middle), and SIDM_3 (right). The densities at 150 pc are estimated by fitting with the NFW profile for the CDM simulation and the Burkert profile for the SIDM_1 and SIDM_3 simulations. The contrast of squares is proportional to the V_{peak} , which is the maximum circular velocity over the subhalo's history. Red filled squares with error bars represent the first and third quartiles of $\rho(150\text{pc})$ in each pericenter bin.

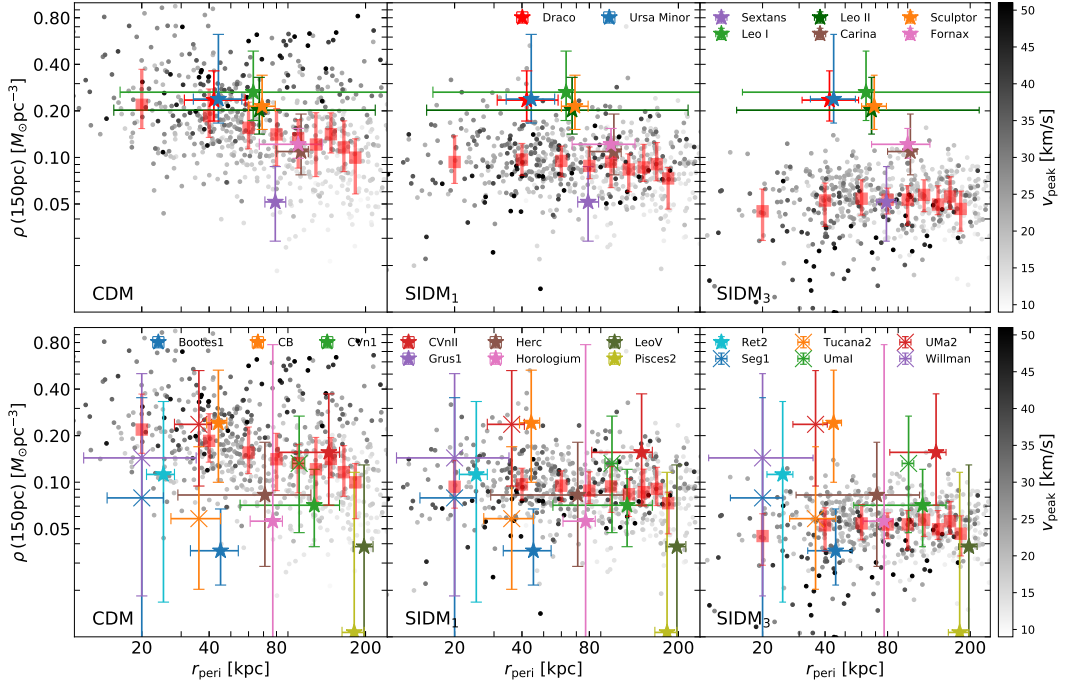


FIG. 2. Same as Fig. 1, but the densities at 150 pc are estimated by fitting with the cuspy profile for all simulations.

highlighting the effect of self-interactions. On the other hand, for subhalos far from the centers of host halos ($130 \text{ kpc} \leq r_{\text{peri}} < 150 \text{ kpc}$), the difference between the CDM and SIDM simulations is much smaller than for the inner regions. Furthermore, we also confirm these trends in other host halos (H2-8), supporting that those are not results of halo-to-halo variations.

Cosmological CDM simulations suggest that subhalos with small r_{peri} are subjected to stronger tidal forces from their hosts than those with large r_{peri} , and thus, less dense subhalos (and also lower V_{peak}) with small r_{peri} could be destroyed [42, 43]. Therefore, there are fewer subhalos with both small r_{peri} and low V_{peak} in the CDM simulation, which is clearly seen in Fig. 1 and 2, and by comparing Fig. 3 and 4. On the other hand, dark matter self-interactions between subhalo's particles work effectively in the dense central region of subhalos with higher V_{peak} for the SIDM cases, and hence, the central densities of such subhalos tend to be lower, and their core tends to be larger. Dark matter self-interactions between subhalo's and host halo's particles could further enhance tidal disruption of subhalos on radial orbits [26]. As a result, since the SIDM subhalos even with higher V_{peak} could be destroyed by tidal effect, the dependence of $\rho(150\text{pc})$ on the pericenter disappears in the SIDM simulations (see Fig. 3 and 4), and the difference between the CDM and SIDM is prominent in subhalos with small pericenter. These results highlight that the Milky-Way satellites with small pericenter are ideal sites to further constrain the nature of dark matter by future large spectroscopic surveys such as PFS [54] and Euclid [55].

IV. DISCUSSION

We discuss two caveats associated with our main results: gravothermal core-collapse and galactic disk. Gravothermal core-collapse can increase the central density of subhalos although we do not observe the sign in our simulations. The Galactic disk potential, which is not included in our simulations, could alter the evolution of subhalos with small pericenter.

A. Gravothermal core-collapse

Dark matter self-interaction leads to an outer heat transfer, thereby inducing gravothermal core-collapse such that the central density increases with time [30, 31, 56]. The core-collapse time scales of halos depend largely on self-interaction cross-section and dynamical evolution of halos. Provided that a halo is isolated and the SIDM cross-section is smaller than $10 \text{ cm}^2\text{g}^{-1}$, the core-collapse cannot occur within the age of Universe. However, subhalos we consider in this work have experienced tidal stripping from the gravitational potential of a host halo. This tidal effect induces the core-

collapse in the central region of subhalos, and the time scale of the core-collapse can be shorter than the age of the Universe, even though the cross-section is smaller than $\sigma/m \sim 3 \text{ cm}^2\text{g}^{-1}$ [31, 57–60]. Nevertheless, there are no such dense subhalos even in the SIDM₃ simulation (Fig. 1 and 2), suggesting that $\sigma/m < 3 \text{ cm}^2\text{g}^{-1}$ is insufficient to induce core-collapse. In the case of $\sigma/m > 3 \text{ cm}^2\text{g}^{-1}$, this process can potentially mitigate the discrepancy between SIDM models and the observed dSphs in $\rho(150\text{pc}) - r_{\text{peri}}$ plane [57, 59, 61]. It, however, is to be noted that it is unclear whether the core-collapse induced by tidal stripping occurs generally. This is because such core-collapse mechanism depends on halo concentration and orbital properties (e.g., eccentricity, pericenter radius, infall time, and so on). Self-interaction between host halo and subhalo particles can alter the abundance and dynamics of subhalos [26]. Although its effect depends on SIDM models and even how self-interaction is implemented in simulations, it could also shorten the timescale of core-collapse. Therefore, we need further studies to assess the impact of core-collapse.

B. Galactic disk

The Galactic disk potential, which is not included in our simulations, could make the inner dark matter potential wall much deeper. Thus, adding a stellar disk preferentially reduces the subhalo densities and the subhalo abundance with smaller pericenter distances (e.g., [62, 63]), depending on the subhalo concentrations and orbital inclinations [57]. In particular, subhalos with pericenter less than $20\sim 30 \text{ kpc}$ is affected, therefore, the overall trend between $\rho(150\text{pc})$ and r_{peri} in each of our simulations should not be altered.

V. CONCLUSIONS

We conducted high-resolution cosmological N -body simulations based on both CDM and SIDM that resolve density structures of the classical dSph and massive UFD scale subhalos. We have quantified the subhalos' central density at 150 pc from the center of each subhalo. Comparing them with observational data, we have found that the SIDM scattering cross-section of $\sigma/m < 3 \text{ cm}^2\text{g}^{-1}$ is favored. Subhalos with higher $\rho(150\text{pc})$ tend to have lower V_{peak} in the SIDM₁ and SIDM₃ simulations, whereas CDM counterparts tend to have higher V_{peak} . This feature is prominent in subhalos with small pericenter due to the combination of hosts' tide and self-interactions. Therefore, the Milky-Way satellites with small pericenter are ideal sites to further constrain the nature of dark matter by future large spectroscopic surveys.

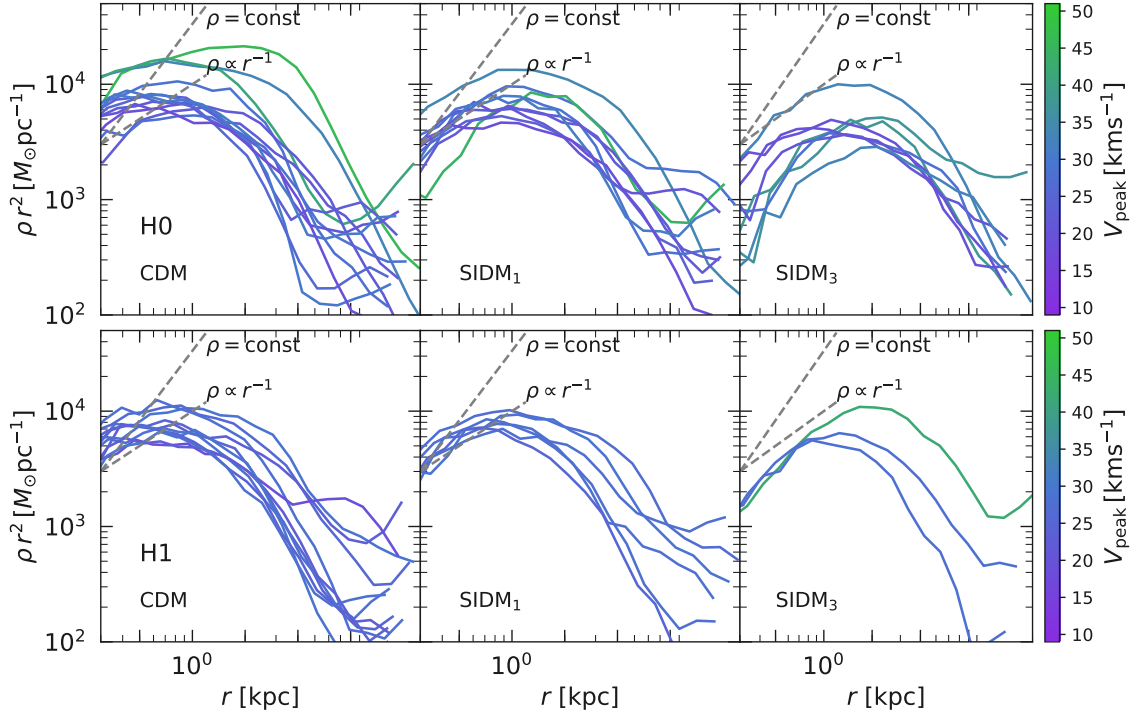


FIG. 3. Density profiles of subhalos with $r_{\text{peri}} < 30$ kpc for CDM (left), SIDM_1 (middle), and SIDM_3 (right). Each curve is colored in proportion to the V_{peak} . Top and bottom panels show the results of subhalos hosted by H0 and H1, respectively.

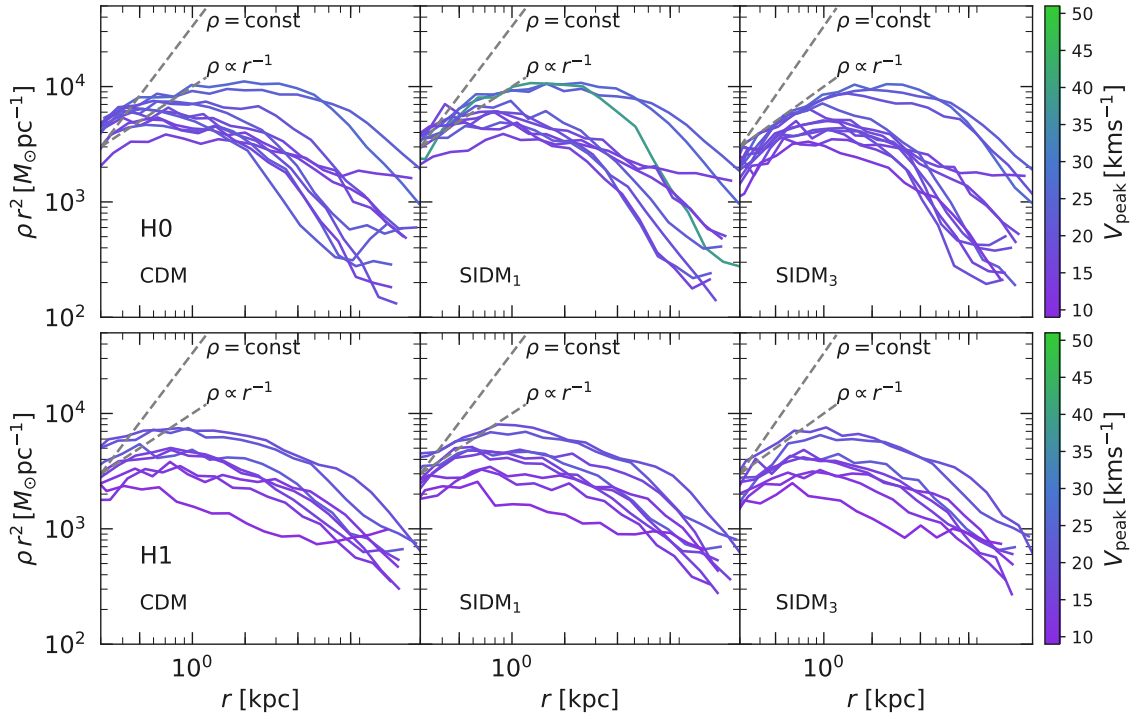


FIG. 4. Same as Fig. 3 but for subhalos with $130 \leq r_{\text{peri}} < 150$ kpc.

ACKNOWLEDGMENTS

We thank Ethan O. Nadler for his helpful discussions. Numerical computations were carried out on Aterui-II supercomputer at the Center for Computa-

tional Astrophysics, National Astronomical Observatory of Japan. This work has been supported by MEXT as “Program for Promoting Researches on the Supercomputer Fugaku” (JPMXP1020200109), and JICFuS. We thank the support of MEXT/JSPS KAKENHI Grant Number JP18H04337, JP20H05245 (for TI), 20H01895, and 21K13909 (for KH).

-
- [1] N. A. Bahcall, J. P. Ostriker, S. Perlmutter, and P. J. Steinhardt, *Science* **284**, 1481 (1999), astro-ph/9906463.
 - [2] M. Tegmark, M. A. Strauss, M. R. Blanton, K. Abazajian, S. Dodelson, H. Sandvik, X. Wang, D. H. Weinberg, I. Zehavi, N. A. Bahcall, et al., *Phys. Rev. D* **69**, 103501 (2004), astro-ph/0310723.
 - [3] V. Springel, C. S. Frenk, and S. D. M. White, *Nature (London)* **440**, 1137 (2006), astro-ph/0604561.
 - [4] R. Mandelbaum, H. Miyatake, T. Hamana, M. Oguri, M. Simet, R. Armstrong, J. Bosch, R. Murata, F. Lanusse, A. Leauthaud, et al., *Publ. of the Astron. Society of Japan* **70**, S25 (2018), 1705.06745.
 - [5] C. Heymans, T. Tröster, M. Asgari, C. Blake, H. Hildebrandt, B. Joachimi, K. Kuijken, C.-A. Lin, A. G. Sánchez, J. L. van den Busch, et al., *Astron. Astrophys.* **646**, A140 (2021), 2007.15632.
 - [6] T. Ishiyama, F. Prada, A. A. Klypin, M. Sinha, R. B. Metcalf, E. Jullo, B. Altieri, S. A. Cora, D. Croton, S. de la Torre, et al., *Mon. Not. R. Astron. Soc.* **506**, 4210 (2021), 2007.14720.
 - [7] DES Collaboration, T. M. C. Abbott, M. Aguena, A. Alarcon, S. Allam, O. Alves, A. Amon, F. Andrade-Oliveira, J. Annis, S. Avila, et al., arXiv e-prints arXiv:2105.13549 (2021), 2105.13549.
 - [8] J. F. Navarro, C. S. Frenk, and S. D. M. White, *Astrophys. J.* **490**, 493 (1997), arXiv:astro-ph/9611107.
 - [9] A. Burkert, *The Astrophysical Journal Letters* **447**, L25 (1995).
 - [10] W. De Blok, A. Bosma, and S. McGaugh, *Monthly Notices of the Royal Astronomical Society* **340**, 657 (2003).
 - [11] S.-H. Oh, W. De Blok, E. Brinks, F. Walter, and R. C. Kennicutt Jr, *The Astronomical Journal* **141**, 193 (2011).
 - [12] S.-H. Oh, C. Brook, F. Governato, E. Brinks, L. Mayer, W. De Blok, A. Brooks, and F. Walter, *The Astronomical Journal* **142**, 24 (2011).
 - [13] K. A. Oman, J. F. Navarro, A. Fattahi, C. S. Frenk, T. Sawala, S. D. M. White, R. Bower, R. A. Crain, M. Furlong, M. Schaller, et al., *Mon. Not. R. Astron. Soc.* **452**, 3650 (2015), 1504.01437.
 - [14] D. N. Spergel and P. J. Steinhardt, *Physical Review Letters* **84**, 3760 (2000).
 - [15] S. Tulin and H.-B. Yu, *Physics Reports* **730**, 1 (2018).
 - [16] J. Zavala, M. Vogelsberger, and M. G. Walker, *Mon. Not. R. Astron. Soc.* **431**, L20 (2013), 1211.6426.
 - [17] O. D. Elbert, J. S. Bullock, S. Garrison-Kimmel, M. Rocha, J. Oñorbe, and A. H. G. Peter, *Mon. Not. R. Astron. Soc.* **453**, 29 (2015), 1412.1477.
 - [18] M. Kaplinghat, S. Tulin, and H.-B. Yu, *Physical Review Letters* **116**, 041302 (2016).
 - [19] S. Y. Kim, A. H. Peter, and D. Wittman, *Monthly Notices of the Royal Astronomical Society* **469**, 1414 (2017).
 - [20] A. Robertson, R. Massey, and V. Eke, *Monthly Notices of the Royal Astronomical Society* **465**, 569 (2017).
 - [21] L. Sagunski, S. Gad-Nasr, B. Colquhoun, A. Robertson, and S. Tulin, *Journal of Cosmology and Astroparticle Physics* **2021**, 024 (2021).
 - [22] A. Loeb and N. Weiner, *Physical Review Letters* **106**, 171302 (2011).
 - [23] M. Vogelsberger, J. Zavala, and A. Loeb, *Mon. Not. R. Astron. Soc.* **423**, 3740 (2012), 1201.5892.
 - [24] X. Chu, C. Garcia-Cely, and H. Murayama, *Phys. Rev. Lett.* **122**, 071103 (2019), 1810.04709.
 - [25] A. Banerjee, S. Adhikari, N. Dalal, S. More, and A. Kravtsov, *J. Cosmology Astropart. Phys* **2020**, 024 (2020), 1906.12026.
 - [26] E. O. Nadler, A. Banerjee, S. Adhikari, Y.-Y. Mao, and R. H. Wechsler, *Astrophys. J.* **896**, 112 (2020), 2001.08754.
 - [27] L. Ackerman, M. R. Buckley, S. M. Carroll, and M. Kamionkowski, *Physical Review D* **79**, 023519 (2009).
 - [28] K. Petraki and R. R. Volkas, *International Journal of Modern Physics A* **28**, 1330028 (2013), 1305.4939.
 - [29] F. Kahlhoefer, K. Schmidt-Hoberg, M. T. Frandsen, and S. Sarkar, *Monthly Notices of the Royal Astronomical Society* **437**, 2865 (2014).
 - [30] S. Balberg, S. L. Shapiro, and S. Inagaki, *Astrophys. J.* **568**, 475 (2002), astro-ph/0110561.
 - [31] H. Nishikawa, K. K. Boddy, and M. Kaplinghat, *Phys. Rev. D* **101**, 063009 (2020), 1901.00499.
 - [32] E. Tollet, A. V. Macciò, A. A. Dutton, G. S. Stinson, L. Wang, C. Penzo, T. A. Gu tcke, T. Buck, X. Kang, C. Brook, et al., *Mon. Not. R. Astron. Soc.* **456**, 3542 (2016), 1507.03590.
 - [33] A. Fitts, M. Boylan-Kolchin, O. D. Elbert, J. S. Bullock, P. F. Hopkins, J. e. Oñorbe, A. Wetzel, C. Wheeler, C.-A. Faucher-Giguère, D. Kereš, et al., *Mon. Not. R. Astron. Soc.* **471**, 3547 (2017), 1611.02281.
 - [34] A. Lazar, J. S. Bullock, M. Boylan-Kolchin, T. K. Chan, P. F. Hopkins, A. S. . Graus, A. Wetzel, K. El-Badry, C. Wheeler, M. C. Straight, et al., *Mon. Not. R. Astron. Soc.* **497**, 2393 (2020), 2004.10817.
 - [35] K. Hayashi, M. Ibe, S. Kobayashi, Y. Nakayama, and S. Shirai, *Phys. Rev. D* **103**, 023017 (2021), 2008.02529.
 - [36] M. Kaplinghat, S. Tulin, and H.-B. Yu, *Phys. Rev. Lett.* **116**, 041302 (2016), 1508.03339.
 - [37] A. Kamada, M. Kaplinghat, A. B. Pace, and H.-B. Yu, *Phys. Rev. Lett.* **119**, 111102 (2017), 1611.02716.
 - [38] M. Valli and H.-B. Yu, *Nature Astronomy* **2**, 907 (2018), 1711.03502.
 - [39] A. Robertson, R. Massey, V. Eke, J. Schaye, and T. Theuns, *Mon. Not. R. Astron. Soc.* **501**, 4610 (2021), 2009.07844.

[40] J. Zavala, M. R. Lovell, M. Vogelsberger, and J. D. Burger, *Phys. Rev. D* **100**, 063007 (2019), 1904.09998.

[41] J. I. Read, M. Walker, and P. Steger, *Monthly Notices of the Royal Astronomical Society* **484**, 1401 (2019).

[42] M. Kaplinghat, M. Valli, and H.-B. Yu, *Mon. Not. R. Astron. Soc.* **490**, 231 (2019), 1904.04939.

[43] K. Hayashi, M. Chiba, and T. Ishiyama, *Astrophys. J.* **904**, 45 (2020), 2007.13780.

[44] M. Crocce, S. Pueblas, and R. Scoccimarro, *Mon. Not. R. Astron. Soc.* **373**, 369 (2006), astro-ph/0606505.

[45] Planck Collaboration, N. Aghanim, Y. Akrami, M. Ashdown, J. Aumont, C. Baccigalupi, M. Ballardini, A. J. Banday, R. B. Barreiro, N. Bartolo, et al., *Astron. Astrophys.* **641**, A6 (2020), 1807.06209.

[46] T. Ishiyama, T. Fukushima, and J. Makino, *Publ. of the Astron. Society of Japan* **61**, 1319 (2009).

[47] T. Ishiyama, K. Nitadori, and J. Makino, in *Proc. Int. Conf. High Performance Computing, Networking, Storage and Analysis, SC'12 (Los Alamitos, CA: IEEE Computer Society Press)*, 5:, (arXiv:1211.4406) (2012), ISBN 978-1-4673-0804-5, URL <http://dl.acm.org/citation.cfm?id=2388996.2389003>.

[48] K. Nitadori, J. Makino, and P. Hut, *New Astronomy* **12**, 169 (2006), arXiv:astro-ph/0511062.

[49] A. Tanikawa, K. Yoshikawa, T. Okamoto, and K. Nitadori, *New Astronomy* **17**, 82 (2012), 1104.2700.

[50] A. Tanikawa, K. Yoshikawa, K. Nitadori, and T. Okamoto, *New Astronomy* **19**, 74 (2013), 1203.4037.

[51] K. Yoshikawa and A. Tanikawa, *Research Notes of the American Astronomical Society* **2**, 231 (2018).

[52] P. S. Behroozi, R. H. Wechsler, and H.-Y. Wu, *Astrophys. J.* **762**, 109 (2013), 1110.4372.

[53] P. S. Behroozi, R. H. Wechsler, H.-Y. Wu, M. T. Busha, A. A. Klypin, and J. R. Primack, *Astrophys. J.* **763**, 18 (2013), 1110.4370.

[54] M. Takada et al., *Publ. of the Astron. Society of Japan* **66**, R1 (2014), 1206.0737.

[55] R. Laureijs et al., arXiv e-prints arXiv:1110.3193 (2011), 1110.3193.

[56] W.-X. Feng, H.-B. Yu, and Y.-M. Zhong, *Astrophys. J. Lett.* **914**, L26 (2021), 2010.15132.

[57] F. Kahlhoefer, M. Kaplinghat, T. R. Slatyer, and C.-L. Wu, *J. Cosmology Astropart. Phys* **2019**, 010 (2019), 1904.10539.

[58] O. Sameie, H.-B. Yu, L. V. Sales, M. Vogelsberger, and J. Zavala, *Phys. Rev. Lett.* **124**, 141102 (2020), 1904.07872.

[59] C. A. Correa (2020), 2007.02958.

[60] A. Kamada, H. J. Kim, and T. Kuwahara, *JHEP* **12**, 202 (2020), 2007.15522.

[61] M. Kaplinghat, M. Valli, and H.-B. Yu, *Mon. Not. Roy. Astron. Soc.* **490**, 231 (2019), 1904.04939.

[62] T. Kelley, J. S. Bullock, S. Garrison-Kimmel, M. Boylan-Kolchin, M. S. Pawlowski, and A. S. Graus, *Mon. Not. R. Astron. Soc.* **487**, 4409 (2019), 1811.12413.

[63] V. H. Robles, T. Kelley, J. S. Bullock, and M. Kaplinghat, *Mon. Not. R. Astron. Soc.* **490**, 2117 (2019), 1903.01469.

[64] M. Rocha, A. H. G. Peter, J. S. Bullock, M. Kaplinghat, S. Garrison-Kimmel, J. Oñorbe, and L. A. Moustakas, *Mon. Not. R. Astron. Soc.* **430**, 81 (2013), 1208.3025.

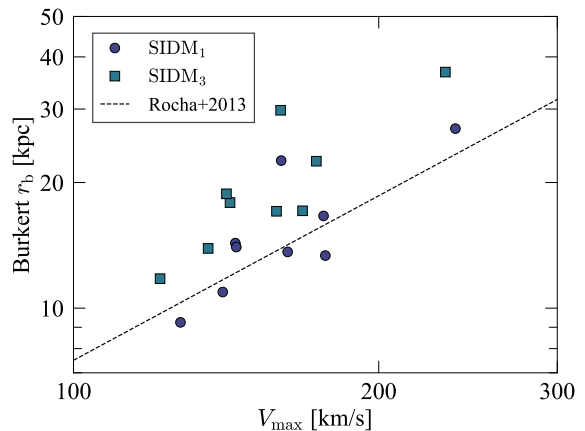


FIG. 5. Burkert scale radius r_b of the nine Milky Way-sized host halos versus their circular velocity peak V_{\max} , for the SIDM_1 and SIDM_3 simulations. Dashed curve is a single power law fitting provided by Rocha et al. [64] from their SIDM_1 simulations, $r_b = 7.50 \text{ kpc} \left(\frac{V_{\max}}{100 \text{ km s}^{-1}} \right)^{1.31}$.

Appendix: Validation of the SIDM implementation

In this section, we validate our SIDM implementation by comparing the size of the SIDM core with a previous study. We fitted the Burkert profile to density profiles of the nine Milky Way-sized host halos from the SIDM_1 and SIDM_3 simulations, and obtained scale radius r_b . Fig. 5 shows r_b versus host halos' circular velocity peak V_{\max} . Our SIDM_1 halos are in good agreement with a previous simulation study [64], and the core size is systematically larger in SIDM_3 halos than in SIDM_1 halos, reinforcing the validity of our SIDM implementation.